

# Quantum Optics Model of Surface Enhanced Raman Spectroscopy for Arbitrarily Shaped Plasmonic Resonators

Mohsen Kamandar Dezfouli and Stephen Hughes  
*Department of Physics, Engineering Physics and Astronomy,  
 Queen's University, Kingston, Ontario, Canada K7L 3N6*  
 (Dated: December 22, 2021)

We present a self-consistent quantum optics approach to calculating the surface enhanced Raman spectrum of molecules coupled to arbitrarily shaped plasmonic systems. Our treatment is intuitive to use and provides fresh analytical insight into the physics of the Raman scattering near metallic surfaces and can be applied to a wide range of geometries including resonators, waveguides, as well as hybrid photonic-plasmonic systems. Our general theory demonstrates that the detected Raman spectrum originates from an interplay between nonlinear light generation and propagation (which also includes the effects of optical quenching). Counter intuitively, at the nonlinear generation stage, we show that the Stokes (anti-Stokes) signal at the molecule location depends on the plasmonic enhancements, through the local density of photon states (LDOS), at the anti-Stokes (Stokes) frequency. However, when propagating from the vibrating molecule to the far field, the Stokes (anti-Stokes) emission experiences a plasmonic enhancement at the Stokes (anti-Stokes) frequency, as expected. We identify the limits of the commonly known  $E^4$  electric-field rule for Raman signal enhancement near plasmonic surfaces at low pump powers, as well as a different  $E^8$  rule at high pump powers, and we clarify the role of the LDOS. Our theory uses a generalized quantum master equation where the plasmonic system is treated as an environmental bath that is described through the photonic Green function of the medium. Therefore, any electrodynamics related physics, such as quenching and propagation, are self-consistently included in the model. The presented formalism is also capable of spatially describing the full Raman response in a simple analytical way, which is typically not possible using simpler coupled mode theories, even if one adopts a quantum picture. This spatial analysis includes both the dependency of the Raman signals at a fixed detector location when the molecule is moved around the plasmonic platform, and the dependency of the Raman signal on the detector location. We demonstrate the power of this approach by using a quasinormal mode expansion theory to construct the photonic Green functions of the plasmonic resonators, and explore several different nanoresonator systems.

## I. INTRODUCTION

Plasmonic devices on the nano scale can be used to enhance the Raman emission from molecules by many orders of magnitude [1–4]. This is greatly appreciated in sensing technologies, as the natural Raman cross sections of different molecules are extremely small. The significant enhancement comes from an ultratight confinement of light that does not suffer from the diffraction limit. Even though the cavity quality factor of typical plasmonic resonances are very low, perhaps on the order of 10, the significant local fields for the plasmonic resonances can lead to very large total spontaneous emission enhancement factors, on the order of 1000 and more. Thus, the plasmonic devices introduce new possibilities for next generation broadband chemical sensors. In terms of design, a variety of different geometries can be used for plasmonic light enhancement such as resonators [5–8], waveguides [9–11], and hybrid photonic-plasmonic systems [12–14] (see Fig. 1 for some typical geometries of interest). Consequently, general theoretical treatments of these devices must be flexible enough to be adopted to a wide range of geometries, possibly with multiple resonances up to even a continuum; while even at the single mode level (which has some conceptual difficulties), a careful treatment of the normalized fields used in a modal analysis is required (e.g., these are not simple leaky cav-

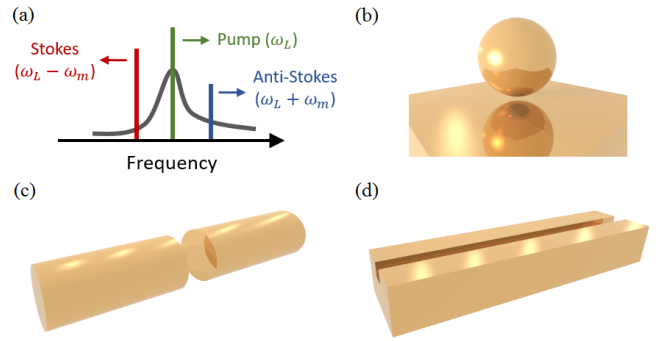


FIG. 1. (a). Picture of the energy levels involved in SERS where a molecule of interest is coupled to a plasmonic environment. The broad, and in general non-Lorentzian, plasmonic response is sketched where the Stokes and anti-Stokes signal are enhanced according to strength of the coupling regime they belong to. (b)-(d). Schematics of example plasmonic structures that can be used to perform SERS.

ity modes because of the material absorption).

In the past, several different approaches have been taken to theoretically study Surface Enhanced Raman Spectroscopy (SERS) in plasmonic geometries, where various ideas and objectives have been drawn [15–22]. For example, density functional theory (DFT) has been

used to successfully calculate the Raman spectra of molecules [17, 20]. This approach can partly capture the effect of the surface roughness of the nanoparticles on SERS, which is particularly important when the molecule gets very close to the metal. On the other hand, if the molecule is too near to the metallic surface (e.g., a few nanometer away), extreme quenching at the metal surface becomes possible which in turn leads to a poor quantum efficiency for photons to propagate out radiatively and be detected. Moreover, the technical difficulty of DFT schemes, along with the significant computational resources required, can impose practical limitations in studying arbitrary geometries, specially when the spatial extent of the device becomes prohibitively large. More recently, a perturbation analysis of SERS has been proposed where the plasmonic system is treated as a quasi-particle [22] and enhancements that are orders of magnitudes larger than what calculated using standard electrodynamics theory, are predicted. While some of the conclusions are somewhat controversial, e.g., the work suggests that chemical enhancement can perhaps be ruled out in plasmonic SERS, the key work is based on using the normal modes for the plasmonic nanoparticles, which are known to be problematic, not only in lossy plasmonic systems but in all open cavity systems in general [23–26].

There has also been a semiclassical study of SERS where only the Raman induced dipole is treated quantum mechanically [19]. This approach has been primarily developed for multilayer dielectric systems and neglects the quantum mechanical interplay between the electromagnetic field and the molecular vibrations, which can be especially important at nonlinear higher pump powers. Such high field regimes are perhaps more feasible using plasmonic systems as typically several orders of magnitudes more enhancements are achievable compared to dielectric systems. In addition to these works, there are recent quantum optomechanical descriptions of SERS in plasmonic systems, where simple phenomenological decay rates are used in a single mode description with Lorentzian line shapes [27, 28]. While these approaches are intuitive, not too complex, and can be in principle be implemented for simple cavity geometries, the computational cost for extending beyond a single mode picture can be prohibitive, arising from the fact that very large Hilbert spaces are commonly needed for converged results. However, if the complexity of having multiple overlapping resonances can be dealt with, such a quantum mechanical picture can lead to a computationally cost-effective model for study of SERS near plasmonic systems with arbitrary geometry, where one can go well beyond an approximate single mode picture.

In this work, we use an open system quantum optics approach to derive analytical expressions for the spatially-dependent detected Stokes and anti-Stokes intensities for molecules coupled to a general plasmonic system. Our results can be directly applied in their current form to arbitrarily shaped geometries (including dielectric systems of course), with no additional computa-

tional cost than calculating the system electromagnetic response which must be done in any case to understand the modal properties of the medium. We use a generalized master equation [29–31] such that the exact system photon Green function is exploited in the formalism, which rigorously includes the full frequency response of the plasmonic enhancement and quenching effects; this avoids having to adopt an approximate coupled mode theory with dissipation, which is usually used in many cavity-QED formalisms, including plasmonic cavity systems.

We start with a representation of the electromagnetic Hamiltonian in the basis of a continuum of quantum field operators, valid for any inhomogeneous lossy medium [32, 33]. Then, the full system dynamics is projected onto the basis of the molecule vibrational mode by tracing out the plasmonic degrees of freedom, treating the plasmonic system as a bath or reservoir, but one that is treated in a self-consistent way. This is expected to be valid as long as the molecule is not strongly coupled to the plasmonic system. Since the molecule vibration or phonon mode is described by a single mode harmonic oscillator, the resulting master equation is of a very simple form that can be solved analytically for different observables of interest, fully including the plasmonic reservoir. In particular, from the obtained master equation, we derive the spectrum analytically, and connect to approximate SERS theories in the literature. In addition, we use our analytical expressions for both Stokes and anti-Stokes intensities to compute a spatial map of the Raman spectrum, either when the molecule is moved nearby the plasmonic system, or when the detector location is scanned. In our main analysis, we consider a gold dimer resonator made of two cylindrical nanorods as shown in Fig. 1.(c) as an example system. However, we stress that no modification to the existing theory is needed for different cavity structures, and one simply requires the Green function for the new system. In order to show such potential for studying arbitrary metal structures, we also consider a hybrid photonic-plasmonic system such that the already mentioned dimer is now placed on top of a photonic crystal nanobeam cavity. This is certainly beyond the usual single mode picture for the photonic medium and demonstrates the generality of our approach.

With regards to SERS, the total Raman signal is known to be partially dependent on the field enhancement at the laser frequency,  $\omega_L$ , as well as field enhancement at the Raman frequency,  $\omega_R$ , through [4]

$$\text{EF}(\omega_R, \omega_L) \propto \frac{|E(\omega_R)|^2 |E(\omega_L)|^2}{|E_0(\omega_R)|^2 |E_0(\omega_L)|^2}, \quad (1)$$

which is most often stated as the  $E^4$  electric-field law for total enhancement, especially when laser and Raman frequencies are close. While our model recovers this general enhancement factor for the detected Raman intensities, our findings shed new light on the details of the Raman process, particularly differentiating between the signal

generating at the molecule location and photon detection on the detectors placed in the far-field. We also show that the  $E^4$  enhancement factor comes from propagation effects at Raman frequencies as well as the LDOS enhancement at the pump frequency, but the Stokes generation is sensitive to the plasmonic local density of states (LDOS) at anti-Stokes frequency and vice-versa, a non-trivial notion that to the best of our knowledge has not been reported before in the literature. In addition, we identify a second (nonlinear) enhancement regime depending on the strength of the pump field. We argue that, for high enough pump intensities, the induced Raman emission enhancement factor can follow a  $E^8$  electric-field rule instead.

The rest of our paper is organized as follows. In Sec. II, we introduce the details of our SERS theory, including the quantized system Hamiltonian in arbitrary dispersive and lossy media; we also present our generalized master equation projected onto the basis of the molecule, and derive the spatially dependent spectrum calculated using the expectation values of two-time correlation functions; in addition, for a localized plasmon resonance, we use the approach of quasinormal modes (QNMs) as a basis to accurately obtain the plasmonic Green function, allowing us to study the spatial dependence of SERS in a remarkably clear and simply way. In the same section, we also briefly discuss the key elements of an alternative quantum optomechanical model using coupled modes for the resonator and a molecule, but restricted to a single plasmon mode picture [28]; we later use this for comparison and verification of our general model in this limit. Next, in Sec. III, we adopt our analytical expression for the Raman spectrum to perform a detailed study of SERS using the two example plasmonic systems mentioned above. Finally, we present our conclusions in Sec. IV.

## II. THEORY

In this section, we present the key elements of our formalism including the system Hamiltonian in quantized form and the generalized master equation which must be solved for the optical spectrum to be obtained. We also briefly discuss the QNM representation of the system Green function that can be used to accurately estimate the emission characteristics of two different plasmonic cavity systems that we study.

### A. System Hamiltonian

The molecular vibration of interest can be considered as a simple Harmonic oscillator, where the corresponding Hamiltonian can be written as

$$H_m = \hbar\omega_m b^\dagger b, \quad (2)$$

where  $b$  and  $b^\dagger$  satisfy the Bosonic commutation relation  $[b, b^\dagger] = 1$  and  $\omega_m$  is the real-valued frequency of the

vibrational mode. In reality, a single molecule supports more than one vibrational mode at different frequencies, however in practice, usually one of them in particular is under investigation. Quite generally, the free field Hamiltonian in a lossy medium can be expressed in terms of a continuum of field operators,  $\mathbf{f}(\mathbf{r}, \omega)$ , such that [32, 33]

$$H_{ph} = \hbar \int d\mathbf{r} \int_0^\infty d\omega \omega \mathbf{f}^\dagger(\mathbf{r}, \omega) \mathbf{f}(\mathbf{r}, \omega), \quad (3)$$

where  $\mathbf{f}$  and  $\mathbf{f}^\dagger$  follow Bosonic algebra with commutation rules,

$$[\mathbf{f}(\mathbf{r}, \omega), \mathbf{f}^\dagger(\mathbf{r}', \omega')] = \mathbf{I} \delta(\mathbf{r} - \mathbf{r}') \delta(\omega - \omega'). \quad (4)$$

Importantly, our picture of the photonic environment is not restricted to a single mode case. As mentioned in the introduction, this is necessary in general, as many plasmonic environments do not satisfy a single mode regime. For example, in case of plasmonic waveguides, naturally there is a continuum of propagating modes involved. In the case of hybrid photonic-plasmonic systems, there are at very least two modes involved. This later case is also true for many plasmonic resonators, especially when small gaps sizes are used, such as the one schematically shown in Fig. 1(b). Even in the single mode regime, plasmonic resonances are described using QNMs that are solutions to a non-Hermitian wave equation, and subsequently the quantization procedure is non trivial. Thus, it is not obvious how one should include the important medium parameters, such as the LDOS, propagation of light from the molecule to detector, as well as quenching in the quantum mechanical theory of SERS. The usefulness of the continuum picture used above becomes further revealed when the electric-field operator for a lossy medium described by the complex permittivity function  $\varepsilon(\mathbf{r}, \omega)$  is expanded in terms of the field operators,  $\mathbf{f}(\mathbf{r}, \omega)$ , using [32, 33]

$$\mathbf{E}(\mathbf{r}, \omega) = \frac{1}{\varepsilon_0} \int d\mathbf{r}' \mathbf{G}(\mathbf{r}, \mathbf{r}'; \omega) \cdot \sqrt{\frac{\hbar \varepsilon_0}{\pi} \text{Im}\{\varepsilon(\mathbf{r}', \omega)\}} \mathbf{f}(\mathbf{r}', \omega), \quad (5)$$

where the two space point classical Green function,  $\mathbf{G}(\mathbf{r}, \mathbf{r}'; \omega)$  is the solution to the classical Helmholtz equation

$$\begin{aligned} \nabla \times \nabla \times \mathbf{G}(\mathbf{r}, \mathbf{r}'; \omega) - \frac{\omega^2}{c^2} \varepsilon(\mathbf{r}, \omega) \mathbf{G}(\mathbf{r}, \mathbf{r}'; \omega) \\ = \frac{\omega^2}{c^2} \mathbf{I} \delta(\mathbf{r} - \mathbf{r}'), \end{aligned} \quad (6)$$

subjected to, in general, open boundary condition. Note that our defining equation for the Green function is slightly different than another commonly used notation [34] in its right hand side. When we derive our master equation below, the plasmonic degrees of freedom will be traced out and effectively the classical Green function,  $\mathbf{G}(\mathbf{r}, \mathbf{r}'; \omega)$ , remains to characterize the plasmonic

behavior in our model. This reservoir is justified as the molecule is typically weakly coupled to the plasmonic system (but in the Purcell regime), especially with their low quality factors.

In a dipole interaction, the induced Raman polarization,  $\mathbf{p}_R$ , can be written as

$$\mathbf{p}_R = \boldsymbol{\alpha}_R \cdot \mathbf{E}(\mathbf{r}_m), \quad (7)$$

where  $\boldsymbol{\alpha}_R$  is the Raman polarizability tensor of the molecule that can be expressed in terms of the well-known Raman tensor of the molecule,  $\mathbf{R}$ , and the quantized displacement via [4]

$$\boldsymbol{\alpha}_R = \mathbf{R} \sqrt{\frac{\hbar}{2\omega_m}} (b + b^\dagger), \quad (8)$$

and  $\mathbf{E}(\mathbf{r}_m)$  is the total electric field operator at the molecule location  $\mathbf{r}_m$ , defined as

$$\mathbf{E}(\mathbf{r}) = \int d\omega \mathbf{E}(\mathbf{r}, \omega) + \text{H.c.} \quad (9)$$

Thus, the interaction Hamiltonian associated with the Raman induced dipole oscillation is

$$H_I = -\mathbf{p}_R \cdot \mathbf{E}(\mathbf{r}_m) \quad (10)$$

$$= -\sqrt{\frac{\hbar}{2\omega_m}} (b + b^\dagger) \mathbf{E}(\mathbf{r}_m) \cdot \mathbf{R} \cdot \mathbf{E}(\mathbf{r}_m). \quad (11)$$

This form of the system Hamiltonian is similar to the (coupled-mode) optomechanical Hamiltonian used in [27, 28], which we discuss in more details in subsection IID; however, here we use a continuum representation of the electromagnetic field, and the classical Green function of the system is incorporated in a self-consistent manner through use of Eq. (5).

## B. Generalized master equation

We now use the above Hamiltonian to show how a generalized master equation can be constructed, when the plasmonic system is treated as a photonic reservoir. To proceed, we note that the Raman scattering mechanism is a nonlinear optical process that the pump field at frequency  $\omega_L$  induces a polarization that oscillates at the Raman frequency,  $\omega_R = \omega_L \pm \omega_m$ . Therefore, it is natural to assume that the  $\mathbf{E}(\mathbf{r}_m)$  on the left side of the Raman tensor in Eq. (11) includes only the pump frequency in its expansion, while the  $\mathbf{E}(\mathbf{r}_m)$  on the right side includes all other frequencies but the pump. In addition, we use a classical representation of the pump field to simplify the mathematics involved, which is valid for the high pump fields of interest; thus for the pump field, we are working with averaged field operators where small quantum mechanical fluctuations are neglected (which is consistent with the fact that the field operators are going to be traced out eventually).

For the initial pump field, we consider a continuous wave (CW) excitation with amplitude  $\mathbf{F}_0$  at frequency  $\omega_L$ . In the presence of the scattering geometry, the pump field at the molecule location is

$$\mathbf{F}_p(\mathbf{r}_m, t) = \eta [\mathbf{F}_0(\mathbf{r}_m) e^{i\omega_L t} + \mathbf{F}_0^*(\mathbf{r}_m) e^{-i\omega_L t}], \quad (12)$$

where  $\eta$  is the external field enhancement factor and can be calculated through use of the system Green function:

$$\eta = 1 + \frac{\int [\varepsilon(\mathbf{r}, \omega_L) - \varepsilon_B] \mathbf{n} \cdot \mathbf{G}(\mathbf{r}_m, \mathbf{r}; \omega_L) \cdot \mathbf{F}_0(\mathbf{r}) d\mathbf{r}}{\mathbf{n} \cdot \mathbf{F}_0(\mathbf{r}_m)}. \quad (13)$$

Here, the unit vector  $\mathbf{n}$  represents the direction of the induced Raman dipole which is determined by the dominant Raman tensor element,  $R_{nn}$ . Note that the value of  $\eta$  implicitly depends on the molecule location,  $\mathbf{r}_m$ , and the laser frequency,  $\omega_L$ . The dielectric function difference involved in this expression, where  $\varepsilon_B$  refers to the background medium, implies that the spatial integration takes place only over the volume of the metallic nanoparticles. Also, note that, we have used  $\mathbf{F}$  for the classical pump field to reserve  $\mathbf{E}$  as a quantum mechanical electric field operator, and  $\mathbf{F}_p$  can be considered as  $\langle \mathbf{E}_p \rangle$ .

The general form of the time local master equation in the interaction picture (tilde represents the interaction picture), using a Born-Markov approximation is [29, 30]

$$\begin{aligned} \frac{\partial \tilde{\rho}(t)}{\partial t} = & -\frac{1}{\hbar^2} \int_0^t d\tau \text{tr}_R \left\{ \left[ \tilde{H}_I(t), \left[ \tilde{H}_I(t-\tau), \tilde{\rho}(t) \rho_R \right] \right] \right\}, \end{aligned} \quad (14)$$

where  $\tilde{\rho}$  is the reduced density matrix in the basis of molecular vibrations,  $\rho_R$  is the plasmonic reservoir density that the trace will be performed over, and  $\tilde{H}_I$  is the interaction Hamiltonian in the interaction picture. Working at optical range of frequencies allows one to use the following bath approximation for the field operators, i.e.,

$$\text{tr}_R \{ \mathbf{f}^\dagger(\mathbf{r}, \omega) \mathbf{f}(\mathbf{r}', \omega') \rho_R \} = 0 \quad (15)$$

$$\text{tr}_R \{ \mathbf{f}(\mathbf{r}, \omega) \mathbf{f}^\dagger(\mathbf{r}', \omega') \rho_R \} = \mathbf{I} \delta(\mathbf{r} - \mathbf{r}') \delta(\omega - \omega'). \quad (16)$$

Transforming the Hamiltonian (11) to the interaction picture, then substituting into the master equation (14), and using the above bath approximations, we obtain the reduced density matrix of the system in the basis of the molecule,

$$\begin{aligned} \frac{\partial \tilde{\rho}}{\partial t} = & J_{\text{ph}}(\omega_L + \omega_m) (2b\tilde{\rho}b^\dagger - b^\dagger b\tilde{\rho} - \tilde{\rho}b^\dagger b) \\ & + J_{\text{ph}}(\omega_L - \omega_m) (2b^\dagger \tilde{\rho}b - bb^\dagger \tilde{\rho} - \tilde{\rho}bb^\dagger), \end{aligned} \quad (17)$$

where  $J_{\text{ph}}$  represents the strength of the plasmonic induced Raman emission. As seen,  $J_{\text{ph}}$  depends on the dominant Raman tensor element,  $R_{nn}$ , the field enhancement factor,  $\eta$ , and—most importantly—the plasmonic

LDOS through

$$J_{\text{ph}}(\omega) \equiv \frac{R_{nn}^2 |\eta|^2 |\mathbf{n} \cdot \mathbf{F}_0|^2}{2\varepsilon_0 \omega_m} \text{Im} \{G_{nn}(\mathbf{r}_m, \mathbf{r}_m; \omega)\}. \quad (18)$$

Note that, in going from Eq. (19) to Eq. (17), the time integral upper limit has been extended to infinity, as the time scale for system changes are assumed to be much longer than its counterpart for the reservoir.

In Eq. (17), the first term represents the Stokes signal (which recall is emitted at  $\omega_L - \omega_m$ ) proportional to  $J_{\text{ph}}(\omega_L + \omega_m)$ , and the second term represent the anti-Stokes signal (emitted at  $\omega_L + \omega_m$ ) proportional to  $J_{\text{ph}}(\omega_L - \omega_m)$ . This means that, at the driving/generation stage, the Stokes emission is governed by the plasmonic enhancements via the projected LDOS at the anti-Stokes frequency and vice-versa; this may seem contrary to the common notion that SERS involves field enhancement at the corresponding frequencies for both Stokes and anti-Stokes signals, and moreover it identifies a different operating regime that can be achieved at high pump powers. As will be discussed later, the commonly seen enhancement factor of Eq. (1) is a consequence of the propagation as well as pump field enhancement in the presence of the scattering geometry, particularly when low pump powers are considered. It is also worth mentioning that such features are not totally surprising in the domain of quantum nonlinear optics, e.g., such a non-trivial LDOS coupling has also been noted for the Mollow triplet spectrum from excited quantum dots coupled to plasmonic resonators, where the center peak width depends only on the LDOS at the two side peaks and not at all on the LDOS at the laser drive frequency [35].

To obtain the full master equation of the system, the coupling of the Raman vibrations to the the thermal environmental bath must be also accounted for. This can be done using additional Lindblad terms associated with thermal dissipation as well as incoherent pumping [28]. Thus, one finally arrives at the following master equation for the complete molecule-plasmonic system:

$$\begin{aligned} \frac{\partial \rho}{\partial t} = & -i\omega_m [b^\dagger b, \rho] \\ & + J_{\text{ph}}(\omega_L + \omega_m) (2b\rho b^\dagger - b^\dagger b\rho - \rho b^\dagger b) \\ & + J_{\text{ph}}(\omega_L - \omega_m) (2b^\dagger \rho b - b b^\dagger \rho - \rho b b^\dagger) \\ & + \gamma_m (\bar{n}^{\text{th}} + 1) (2b\rho b^\dagger - b^\dagger b\rho - \rho b^\dagger b) \\ & + \gamma_m \bar{n}^{\text{th}} (2b^\dagger \rho b - b b^\dagger \rho - \rho b b^\dagger), \end{aligned} \quad (19)$$

where the overhead tilde is removed now, as we have moved back to the Schrodinger picture. This generalized master equation can be used to evaluate the time dependence of different operators of interest. In particular, to connect to the Raman detection experiments, this is used in next to obtain an analytical expression for the spatially dependent spectrum.

### C. Detected spectrum on a point detector

The detectable spectrum at  $\mathbf{R}$  is defined as

$$S(\mathbf{R}, \omega) \equiv \langle \mathbf{E}^\dagger(\mathbf{R}, \omega) \cdot \mathbf{E}(\mathbf{R}, \omega) \rangle, \quad (20)$$

where we assume a point detector. The molecule polarization emission transfers to this point (typically in the far field, but not necessarily so) through the system Green function using [36]

$$\mathbf{E}(\mathbf{R}, \omega) = \frac{1}{\varepsilon_0} \mathbf{G}(\mathbf{R}, \mathbf{r}_m; \omega) \cdot \mathbf{p}_R(\mathbf{r}_m; \omega), \quad (21)$$

which is an exact input-output expression that is derived for the Heisenberg equations of motion. Therefore, using the field operator and the molecular polarization definitions, we find

$$S(\mathbf{R}, \omega) = \frac{\hbar R_{nn}^2 |\eta|^2 |\mathbf{n} \cdot \mathbf{F}_0|^2}{2\omega_m \varepsilon_0^2} |\mathbf{G}(\mathbf{R}, \mathbf{r}_m; \omega) \cdot \mathbf{n}|^2 S_0(\omega), \quad (22)$$

where  $S_0(\omega) = S_0^{\text{st}}(\omega) + S_0^{\text{as}}(\omega)$  is the spectrum calculated using the molecule dynamics that is a sum of Stokes,  $S_0^{\text{st}}(\omega)$ , and anti-Stokes,  $S_0^{\text{as}}(\omega)$ , signals, defined from

$$S_0^{\text{st}}(\omega) \equiv \langle b(\omega) b^\dagger(\omega) \rangle \quad (23)$$

$$= \text{Re} \left\{ \int_0^\infty d\tau e^{i(\omega - \omega_L)\tau} \langle b(t) b^\dagger(t + \tau) \rangle \right\}, \quad (24)$$

and

$$S_0^{\text{as}}(\omega) \equiv \langle b^\dagger(\omega) b(\omega) \rangle \quad (25)$$

$$= \text{Re} \left\{ \int_0^\infty d\tau e^{i(\omega - \omega_L)\tau} \langle b^\dagger(t) b(t + \tau) \rangle \right\}. \quad (26)$$

Here, we have excluded  $\langle b(\omega) b(\omega) \rangle$  and  $\langle b^\dagger(\omega) b^\dagger(\omega) \rangle$  terms as they are associated with higher order Raman intensities. Using the quantum regression theorem [29], equations of motion for the two-time expectation values can be derived from the generalized master equation of Eq. (19), which in turn can be solved analytically using Laplace transform techniques to arrive at

$$\begin{aligned} S_0^{\text{st}}(\omega) = & \text{Re} \left\{ \frac{i [\gamma_m (\bar{n}^{\text{th}} + 1) + J_{\text{ph}}(\omega_L + \omega_m)]}{[\omega - (\omega_L - \omega_m) + i(\gamma_m + \Delta J_{\text{ph}})] (\gamma_m + \Delta J_{\text{ph}})} \right\}, \end{aligned} \quad (27)$$

$$\begin{aligned} S_0^{\text{as}}(\omega) = & \text{Re} \left\{ \frac{i [\gamma_m \bar{n}^{\text{th}} + J_{\text{ph}}(\omega_L - \omega_m)]}{[\omega - (\omega_L + \omega_m) + i(\gamma_m + \Delta J_{\text{ph}})] (\gamma_m + \Delta J_{\text{ph}})} \right\}, \end{aligned} \quad (28)$$

where for convenience we have defined  $\Delta J_{\text{ph}} = J_{\text{ph}}(\omega_L + \omega_m) - J_{\text{ph}}(\omega_L - \omega_m)$ . Therefore, we have succeeded in deriving a transparent analytical solutions to the SERS spectrum for any plasmonic system, provided

by Eqs. (22), (27) and (28); by including the classical system Green function for the electromagnetic field, this approach brings considerable power to the existing theory compared to the previous theories.

Before presenting some representative calculations, we first discuss some of the aspects of the analytical SERS spectrum obtained using our generalized Master equation. We begin with the effect of increasing the pump power on the Raman intensities. Let us consider the Stokes emission given in Eq. (27) for two different cases: (i) low pump limit where the thermal pumping quantified by  $\gamma_m (\bar{n}^{\text{th}} + 1)$  is dominant over plasmonic drive  $J_{\text{ph}} (\omega_L + \omega_m)$ ; and (ii) high pump limit where plasmonic induced emission become comparable to or stronger than thermal phonons. Similar conclusions hold for the anti-Stokes signal given in Eq. (28). In the former scenario, the counter-intuitive enhancement process explained earlier remains unseen, and ignored in most works on SERS, especially because the very low values for the Raman tensor elements lead to small  $J_{\text{ph}}$  values. In such cases, the maximum Stokes generation is approximately

$$S_0^{\text{st}} (\omega_L - \omega_m) \cong \frac{\bar{n}^{\text{th}} + 1}{\gamma_m}, \quad (29)$$

where essentially the Stokes generation becomes weakly dependent on the plasmonic enhancement. On the other hand, with the strong modal enhancements possible in plasmonic systems, sufficiently large values for the quantity  $J_{\text{ph}}$  can be obtained such that the Stokes generation is mainly derived by the plasmonic enhancement rather than thermal vibrations. Assuming that  $\Delta J_{\text{ph}}$  is small compared to  $\gamma_m$ , then the maximum Stokes generation is now approximately

$$S_0^{\text{st}} (\omega_L - \omega_m) \cong \frac{J_{\text{ph}} (\omega_L + \omega_m)}{\gamma_m^2}. \quad (30)$$

This is a regime where there is a strong interplay between the plasmonic resonator and the molecular vibrations. The plasmonic enhancement enters in a much stronger fashion through use of Eq. (18). Such nonlinear interplay between the plasmonic resonator and the Raman vibrations has been only recently numerically predicted to be responsible for blue-shifting the peak of the anti-Stokes intensity at high pump powers [28]. Here, we explain the physics behind such an interplay.

Next, we emphasize that the classical system Green function basically enters our formalism twice; once, depending on the pump strength, possibly at the generation stage where Stokes and anti-Stokes emissions are influenced by the dressed-state sampling the plasmonic resonance at their co-frequencies, and then at the propagation stage where the generated Stokes and anti-Stokes photons propagate to the far-field through the plasmonic resonance at their corresponding frequencies. This later effect, along with the effective field enhancement at laser frequency enforced by  $\eta$ , recovers the well-known  $E^4$  enhancement rule for SERS at low pump powers and leads

to the much stronger  $E^8$  enhancement rule at high pump power. This is hidden in our notation using the system Green function, but will become more transparent in subsection II E.

In addition, because the propagation effects are self-consistently included in the definition of the system Green function (including any quenching effects), there is no need for phenomenological effects to be added by hand. For example, the  $\omega^4$  dependence for the detected spectrum considered in [28] comes from a simple dipole emission power argument, whereas in approach it is automatically captured and accounted for in our formulation. Along the same lines, our theory includes the location information of the molecule as well as the detector. Therefore, Stokes and anti-Stokes detectable intensities can be both mapped out when either the molecule or the detector position is changed.

#### D. Coupled-mode quantum optomechanical model

In this subsection, we briefly present the key elements of the normal mode quantum optomechanical studies of SERS, elegantly introduced in Refs. [27, 28], to help the reader compare to our new generalized master equation approach and also to use later to compare the results of the two methods. The starting point is the following quantum mechanical Hamiltonian

$$H = \hbar \omega_c a^\dagger a + \hbar \omega_m b^\dagger b + \hbar g a^\dagger a (b + b^\dagger) + i \hbar \Omega (a e^{i \omega_L t} - a^\dagger e^{i \omega_L t}), \quad (31)$$

where  $a$  and  $a^\dagger$  are the plasmonic ladder operators that follow the Bosonic commutation relation  $[a, a^\dagger] = 1$ . Also,  $g$  is the coupling factor between the single mode plasmonic system and the molecule, and  $\Omega$  is the pump parameter for the plasmonic system. This Hamiltonian can be summed over multiple resonances when necessary, however the numerical/analytical implementations can be cumbersome. More importantly, it is not obvious how one would adopt such an approach to a continuum of modes such as in waveguides.

The corresponding master equation to be solved for system dynamics is

$$\begin{aligned} \frac{d\rho}{dt} = & -\frac{i}{\hbar} [H, \rho] \\ & + \gamma_c (2a\rho a^\dagger - a^\dagger a \rho - \rho a^\dagger a) \\ & + \gamma_m (\bar{n}^{\text{th}} + 1) (2b\rho b^\dagger - b^\dagger b \rho - \rho b^\dagger b) \\ & + \gamma_m \bar{n}^{\text{th}} (2b^\dagger \rho b - b b^\dagger \rho - \rho b b^\dagger). \end{aligned} \quad (32)$$

One then calculates the cavity emitted spectrum using

$$S(\omega) = \omega^4 \text{Re} \left[ \int_0^\infty d\tau e^{i(\omega - \omega_L)\tau} \langle a^\dagger(t) a(t + \tau) \rangle \right], \quad (33)$$

where the quantum regression theorem is employed to find the expectation value of the two-time correlation

function  $\langle a^\dagger(t) a(t+\tau) \rangle$ . In general, numerical simulations of these problems are used to obtain the spectrum. However, if the so-called linearization procedure is used [28, 37] such that the evolution of the operators follow a set of linearly coupled equations one can tackle the problem analytically using the L transform. The later approach is what we do in the results section to compare with our generalized equation technique for the plasmonic reservoir. To make a fair comparison, as the classical pump limit that we employed in our theory is essentially equivalent to the linearized Hamiltonian [28]. Note, also, that the truncation defined in this approach does not include the propagation effects and the additional  $\omega^4$  is used to accommodate a simple dipole propagation argument in the far field. In our approach, the details of radiation propagation are fully included.

### E. QNM expansion of the Green function

In this subsection, we briefly discuss the QNM expansion technique for the Green function that can be used in a general open cavity systems, even for plasmonic resonators. While this provides a powerful tool in analyzing the system response in plasmonic resonators in an efficient manner, it can also be used to simplify our analytically derived SERS spectrum and, e.g., reveal the limits of the well-known  $E^4$  enhancement factor. Extension of the arguments made below to other plasmonic structures such as waveguides and slabs is straightforward, when the appropriate alternative Green function expansion is used.

Quasinormal modes,  $\tilde{\mathbf{f}}_\mu(\mathbf{r})$ , are solutions to a non-Hermitian Maxwell's problem subjected to open boundary conditions. Consequently, they are described by complex frequencies  $\tilde{\omega}_\mu = \omega_\mu - i\gamma_\mu/2$ , where the imaginary part of which is a measure of losses involved, which can be due to leakage of energy from the resonator as well as metallic Ohmic losses. The analytical system Green function can be expanded in terms of these QNMs through [25, 38]

$$\mathbf{G}^{\text{QNM}}(\mathbf{r}_1, \mathbf{r}_2; \omega) = \sum_\mu A(\omega) \tilde{\mathbf{f}}_\mu(\mathbf{r}_1) \tilde{\mathbf{f}}_\mu(\mathbf{r}_2), \quad (34)$$

where  $A(\omega) = \omega^2/2\tilde{\omega}_\mu(\tilde{\omega}_\mu - \omega)$  and  $\tilde{\mathbf{f}}_\mu(\mathbf{r})$  are normalized. The Green function enables us to connect to a wide range of physical quantities such as the spontaneous emission enhancement and non-radiative decay rates from quantum emitters. Normalization of the QNMs can be done in different ways [24, 26]. Note that the Green function expansion in here is different from standard expansions seen in Hermitian theories along with the fact that a complex pole is involved in the QNM expansion.

As an example resonator system, we first consider a gold dimer where each nanorod is made of a cylinder with radius of  $r_r = 10$  nm and height of  $h_r = 80$  nm;

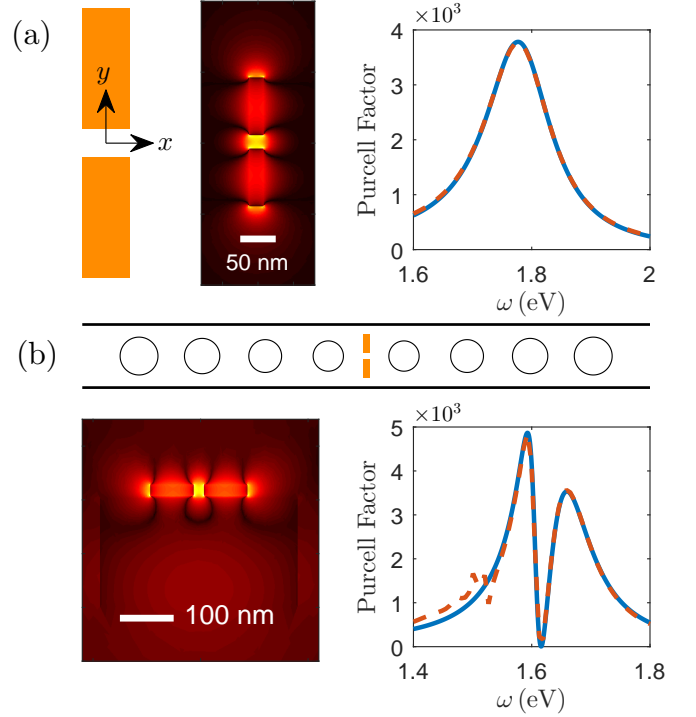


FIG. 2. (a) Two cylindrical nanorods made of gold are used to form a single mode plasmonic resonator. The three sub-figures show the dimer schematic, projected on  $xy$  plane, the spatial map of the dimer QNM, also on the  $xy$  plane, and the projected Purcell enhancement along the  $y$  axis at exactly the middle of the dimer gap. (b) The previous dimer is placed on top of a photonic crystal nanobeam cavity and 5 nm away from the surface of the beam to form a hybrid system. The three sub-figures show the top view of the hybrid device, projected on  $xy$  plane, the spatial map of one of the system QNMs, on the  $yz$  plane, and the projected Purcell enhancement along the  $y$  axis at exactly the middle of the dimer gap. Here, blue-solid is calculated using the QNM expansion of the Green function where the red-dashed is the full dipole calculations.

see Fig. 2.(a). The dimer is placed in free space and the Drude model is used to model its dispersive and lossy behavior through

$$\varepsilon(\omega) = 1 - \frac{\omega_p^2}{\omega(\omega + i\gamma_p)}, \quad (35)$$

where the plasmon frequency and the collision rate are  $\omega_p = 8.29$  eV and  $\gamma_p = 0.09$  eV, respectively. In the same figure we have also plotted the spatial map of the QNM supported by the system where a hot spot is formed in between the 20 nm gap of the dimer. In addition, we have also plotted the corresponding LDOS at exactly the center of the dimer gap and projected along the  $y$ -axis, which shows a single mode behavior over a wide range of frequencies centered at  $\omega_c = 1.78$  eV with the quality factor of  $Q = 13$ . The details of the QNM calculation are presented in Ref. [39].

Next, we place the exact same dimer on top of a

photonic crystal nanobeam cavity to create a hybrid photonic-plasmonic system with multimode characteristics, as schematically shown in Fig. 2.(b). The nanobeam PC-cavity, previously studied in [39], is modeled as silicon-nitride with refractive index of  $n = 2.04$ , where the height of  $h_b = 200$  nm, and the width of  $W_b = 367$  nm. This design uses a mirror section as well as a taper section, the details of which are given in [39], to obtain a large quality factor of  $Q = 3 \times 10^5$  at the resonance frequency of  $\omega_c = 1.62$  eV. Due to the coupling between the dimer and PC-cavity, very strong hybridization of the individual mode takes place. The resonance frequencies of the two hybridized QNMs are found to be  $\omega_1 = 1.64$  eV and  $\omega_2 = 1.61$  eV, with the corresponding quality factors of  $Q_1 = 15$  and  $Q_2 = 55$ , respectively. In Fig. 2.(b), we plot the spatial map of the first QNM with a lower  $Q$ , where a clear signature of hybridization of the individual modes is seen; the same feature was also seen for the other QNM with the higher  $Q$ . When both of the hybrid system QNMs are used, an accurate representation of the system LDOS is obtained over a wide range of frequencies as shown in the same figure. The most important feature of the hybrid LDOS is the interference between the two main QNMs that results in a strong modification of the spontaneous emission rate of a quantum emitter at that place, such that there will be minimum that the emission is significantly reduced (to around 5) [39].

We can now use the QNM representation of the system Green function discussed above to extract the  $E^4$  dependence of our analytical expression for the SERS spectrum that is always present in both of the pump power regimes discussed before. The first key element in Eq. (22) is the enhancement at pump frequency through  $\eta$ . Without loss of generality, we consider the Green function expansion of Eq. (34) when only one QNM is present, namely  $\tilde{\mathbf{f}}(\mathbf{r})$ . Using this approximation, and assuming that the initial pump field is launched along  $\mathbf{n}$ ,  $\eta$  can be written as

$$\eta = A(\omega_L) \left[ \mathbf{n} \cdot \tilde{\mathbf{f}}(\mathbf{r}_m) \right] \left\{ \int [\varepsilon(\mathbf{r}, \omega_L) - \varepsilon_B] \tilde{\mathbf{f}}(\mathbf{r}) d\mathbf{r} \right\}, \quad (36)$$

where  $A(\omega_L)$  can be thought the resonator quality factor,  $Q$ , especially when on resonance, and the spatial integration incorporates a spatial integration over the mode. Importantly, when used in Eq. (22), the modal field value at the molecule location,  $\tilde{\mathbf{f}}(\mathbf{r}_m)$ , recovers the squared dependence of the SERS spectrum at the laser frequency.

Next, we consider the propagation effect through  $|\mathbf{G}(\mathbf{R}, \mathbf{r}_m; \omega) \cdot \mathbf{n}|^2$ . This can be expanded using the system Green function, to find

$$\mathbf{G}(\mathbf{R}, \mathbf{r}_m; \omega) \cdot \mathbf{n} = A(\omega) \tilde{\mathbf{f}}(\mathbf{R}) \left[ \tilde{\mathbf{f}}(\mathbf{r}_m) \cdot \mathbf{n} \right], \quad (37)$$

where  $\tilde{\mathbf{f}}(\mathbf{R})$  is the modal value at the point detector, and  $\tilde{\mathbf{f}}(\mathbf{r}_m) \cdot \mathbf{n}$  is the modal value at the molecule location that appeared before inside  $\eta$ . Taking everything into account, one recovers the well-known power of four rule,  $|\tilde{\mathbf{f}}(\mathbf{r}_m)|^4$ , for the detected SERS spectrum.

Similar consideration can be easily made for the imaginary part of the Green function at the molecule location,  $\text{Im}\{G_{nn}(\mathbf{r}_m, \mathbf{r}_m; \omega)\}$ , to find that  $J_{\text{ph}}$  defined in Eq. (18) is also proportional to  $|\tilde{\mathbf{f}}(\mathbf{r}_m)|^4$ . Therefore, at the high pump powers discussed before, we now find that Raman signal enhances as  $|\tilde{\mathbf{f}}(\mathbf{r}_m)|^8$  instead of  $|\tilde{\mathbf{f}}(\mathbf{r}_m)|^4$ .

### III. RESULTS

We now present some example results of our SERS theory using the plasmonic environments discussed previously. Our analysis will include the role of propagation on the detected Stokes and anti-Stokes signals for different pump scenarios, the effect of pump detuning from the plasmonic resonances on the detectable intensities, as well computing the spatial map of the Stokes (anti-Stokes) intensity profiles. For the molecular vibrations, we use the particular mode of the R6G molecule at  $\omega_m = 0.16$  eV [40] where the thermal dissipation rate is taken to be  $\gamma_m = 1.6$  meV.

We begin by discussing the propagation affects on the detected spectrum. The spectrum calculated using Eqs. (22), (27) and (28) is plotted in Fig. 3 for three different excitation scenarios, where in each case, both the emitted spectrum quantified using  $S_0(\omega)$  (left column) and the detected spectrum—quantified using  $S(\mathbf{R}, \omega)$  when the detector placed  $x = 500$  nm away from the dimer (right column)—are presented (the results are qualitatively the same for larger distances). The three scenarios are as follows: (a)/(d)  $\omega_L = \omega_c$ , where the pump laser is on-resonance with the plasmonic mode, (b)/(e)  $\omega_L = \omega_c + \omega_m$ , where the laser pump is detuned to the blue side of the plasmonic resonance by exactly the frequency of R6G vibration, and finally (c)/(f)  $\omega_L = \omega_c - \omega_m$ , where the laser pump is detuned to the red side of the plasmonic resonance by exactly the frequency of R6G vibration. All the calculation assume room temperature where  $n^{\text{th}} = 0.002$ , and the same fixed value for the pump intensity. As discussed in the theory section, the spectral properties of the Raman signals at the generation stage can be quite different to those that are detected. In particular, the difference depends on the operating frequency for the pump field and the changes of the LDOS between the laser drive frequency and at the Raman sidebands. For example, by comparing Fig. 3.(a) and Fig. 3(d), where the system is pumped on resonance with the plasmonic mode, the propagating effect to the far-field seems to be a bit in favor of more enhancement for the anti-Stokes signal than the Stokes signal. This difference becomes even more pronounced when one excites the system in a red detuning configuration where the anti-Stokes emission exploits the maximum enhancement from the plasmonic environment through propagation. Indeed, in the far-field the anti-Stokes can gain a higher value than the Stokes intensity under high pump intensity that are not shown.

Next, we consider the effect of laser detuning from the

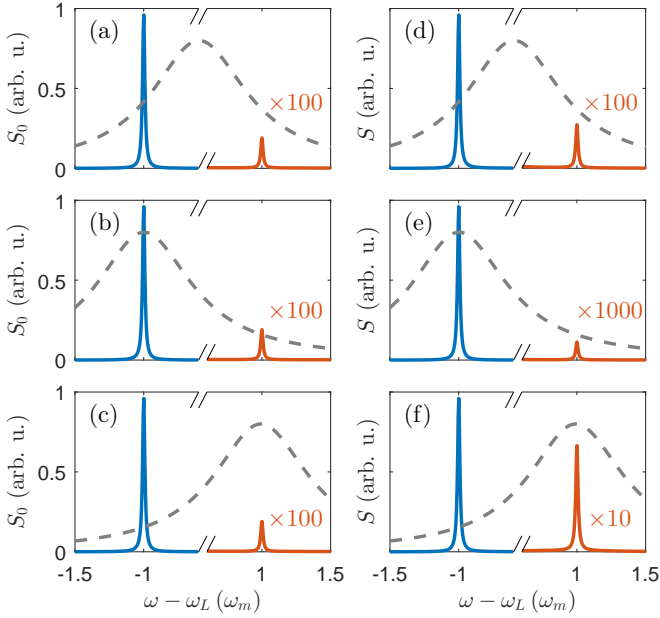


FIG. 3. Raman spectra calculated for the R6G molecule coupled to the gold dimer, using Eq. (22) for three different laser pump frequencies: (a)/(d) where  $\omega_L = \omega_c$ , (b)/(e) where  $\omega_L = \omega_c + \omega_m$  and (c)/(f) where  $\omega_L = \omega_c - \omega_m$ . The plots on the left only show the  $S_0(\omega)$  (emitted spectrum), where in contrast, on the right, the full far-field (detected) spectrum is plotted. The same pump power,  $\epsilon_0 c |\mathbf{F}_0|^2 / 2 = 130 \text{ mW}/\mu\text{m}^2$ , and the temperature,  $T = 300 \text{ K}$ , is assumed in all calculations. The gray-dashed line on the background of all plots indicates the LDOS profile of the plasmonic resonance, and the magnifying factors are only applied to the anti-Stokes intensities.

plasmonic resonance on the Stokes and anti-Stokes intensities. Different cases are considered in Fig. 4, where the Stokes and anti-Stokes signal are calculated as follows: (a) using the quantum optomechanical description briefly discussed in subsection IID for the R6G molecule coupled to the gold dimer, (b) using our analytical expression for the detectable spectrum given in Eq. (22) where the gold dimer Green function is accurately calculated using the QNM expansion of Eq. (34). As seen, the agreement between the two methods is qualitatively good, since the response of the system happens to be very similar to a Lorentzian lineshape, but there are still quantitative differences. Based on our investigations, we attribute these differences to our estimation of the pump enhancement effect which involves calculating  $\eta$  through use of Eq. (13), which in turn employs the full system Green function. To make this clearer, we note an excellent agreement between the prediction of our model and the modal quantum optomechanical model of Ref. [28], if  $\eta$  was estimated using the plasmonic LDOS (which is implied in the theory we compare with) rather than using Eq. (13).

In addition, we further consider three different pump intensity scenarios in Fig. 4(c). As seen, for the the R6G

molecule coupled to the gold dimer, increasing the pump field reshapes the anti-Stokes signal such that a single peak feature at a different location is obtained. For the same pump values, small changes to the general shape of the Stokes signal was noticed. A similar finding was made in [28] suggesting that increasing the pump intensity moves the anti-Stokes signal peak toward the Stokes signal peak in a Raman experiment, due to the nonlinear interactions. Even though this effect is attributed to the nonlinear behavior under intense pumps, note that the  $J_{\text{ph}}$  terms in our master equations are proportional to square of the pump field in comparison to the thermal dissipation terms, and it is important to appreciate the fact that the Raman spectrum is being generated differently than to what is measured in a plasmonic environment. Therefore, the counter intuitive enhancement mechanism argued before is what leads to the generally expected SERS spectrum, where the detuning dependencies of Raman signals for different pump values are correctly captured. Indeed, the results argued earlier would have not been obtained if one used an alternative argument. It is also worth noting that the pump values used in Fig. (4) are such that  $\epsilon_0 c |\mathbf{F}_0|^2 / 2 = 1.3 \times 10^5 \text{ W}/\mu\text{m}^2$  which is extremely high. This is particularly due to lower plasmonic enhancement achieved in using the gold dimer, e.g., in comparison to what used in [28], where a mode volume orders of magnitude smaller than what we have used here is considered. Accordingly, our estimation of the coupling factor  $g$  used in the optomechanical Hamiltonian of Sec. IID for our gold dimer is five orders of magnitude smaller than what used in [28].

Next we demonstrate that our theory can easily be applied to more complex plasmonic environments where the simple single mode (Lorentzian-like) picture does not work. Such a task is not easy using a coupled mode quantum theory for computing the SERS, even if several modes were employed. For example, even ignoring the conceptual difficulties of treating the plasmon mode as a normal mode, numerical quantum mechanical calculation of the SERS when there are three modes involved, one for the molecule and two for the resonator, can be numerically cumbersome, since typically the size of the truncated Hilbert space depends strongly on the number of modes involved (each one quantized) and therefore obtaining converged are highly computationally demanding. In contrast, our theory in its existing form is capable of overcoming such challenges.

As an example non-single mode system, we consider the hybrid photonic-plasmonic structure discussed in Sec. IIE. Because the hybrid structure supports more than one QNMs, the resulting spectrum can be naturally different. In particular, one might wonder if there are certain aspects of the Raman process that is derived by one particular QNM. Using the analytical results or our theory, Eq. (22), and the QNM representation of the system Green function for the hybrid system through expansion of Eq. (34), we plot the Stokes (blue-solid) and anti-Stokes (red-dashed) detected intensities for different

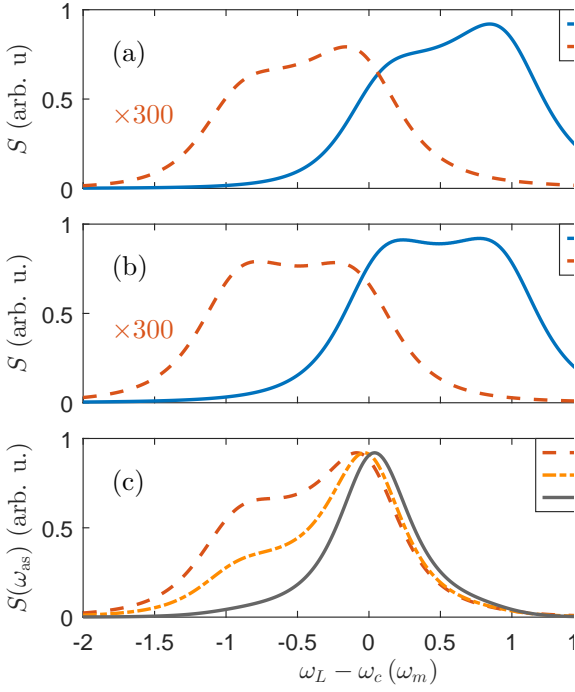


FIG. 4. Plot of Stokes and anti-Stokes intensity calculated as a function of laser detuning when: (a) T monic dimer is assumed to be having a Lorentzian line shape and the quantum optomechanical model of subsection IID is used where the pump power is set to  $\Omega = 1$  eV. (b) The true gold dimer response is used through inclusion of the system Green function in Eq. (22) and the pump power is set to  $\varepsilon_0 c |\mathbf{F}_0|^2 / 2 = 130 \text{ mW}/\mu\text{m}^2$  where using the recipe in Ref. [28] translates to approximately  $\Omega = 1$  eV. (c) Shows the effects of increasing the pump intensity on the anti-Stokes detectable intensities when going from red-dashed to gray-solid using our generalized Master equation technique. The Stokes signals were quite similar when the pump intensity was increased and the starting pump power is set to  $\varepsilon_0 c |\mathbf{F}_0|^2 / 2 = 130 \text{ kW}/\mu\text{m}^2$ .

pump detuning in Fig. (5). These results are displayed in two different ways: (a) the detuning is with respect to the first hybrid resonance at  $\omega_1 = 1.64$  eV that is associated with the lower  $Q$  QNM, and is confirmed to be more dimer-like; (b) detuning is quantified with respect to the second hybrid resonance at  $\omega_2 = 1.61$  eV, that is associated with the higher  $Q$  QNM, and is confirmed to be less dimer-like. We have also projected the hybrid LDOS on the background in gray dotted-dashed for guidance. As seen, when the LDOS is suppressed to near zero due to the interference between the QNMs, the Raman intensities follow the same trend. In addition, there seems to be three high intensity operation points available for both Stokes and anti-Stokes detections. More importantly, the maximum detection seems to be one  $\omega_m$  to the right (left) for the Stokes (anti-Stokes) in Fig. (5)(b) where the detuning is being measured with respect to the  $\omega_2$ . Therefore, in this specific configuration of the hybrid system, the SERS signals seem to be coupled to the QNM fre-

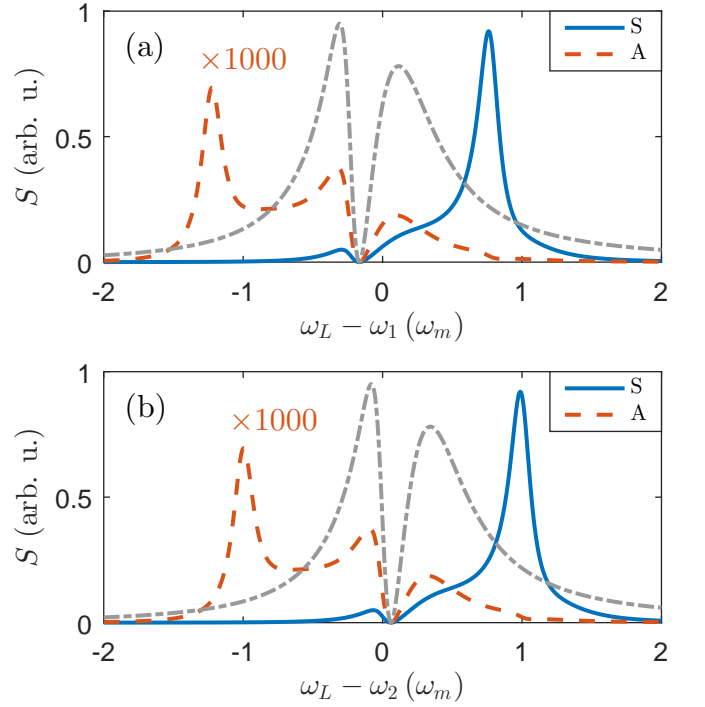


FIG. 5. Stokes (blue-solid) and anti-Stokes (red-dashed) detection intensities for the R6G molecule when coupled to the hybrid device at exactly the middle of the dimer gap and oriented along the y axis. The plasmonic LDOS is projected in gray in the background for comparison. (a) and (b) show representation of the same data for when the laser detuning is measured with respect to  $\omega_1$  and  $\omega_2$ , respectively.

quency  $\omega_2$  that is primarily attributed to the nanobeam cavity resonance rather than the gold dimer. This is not a general conclusion to be made and for different configurations of the hybrid device, depending on the regime where the two QNMs are coupled [39], other outcomes might be feasible.

Our model also allows accurate and rapid calculation of both Stokes and anti-Stokes intensities as a function of the spatial location both for the molecule and for the detector. Although, previous theories can effectively employ a position dependent coupling factor for the molecule at different location in order to attempt such scenarios, this can be numerically inefficient specially when multiple resonances are involved, for the reasons elaborated before. We will demonstrate this below for the single mode gold dimer. Assuming that the detection setup is fixed at a particular location (far from the dimer), one can move the molecule around the plasmonic resonator and see how both Stokes and anti-Stokes emissions are dependent upon that. In Fig. 6.(a), we have plotted such a map only for Stokes intensity (the profile is confirmed to be the same for anti-Stokes but having relatively lower values for the condition under investigation) which confirms that the Raman emission is dominated by the modal shape of the plasmonic mode, namely the Purcell factor behavior of a quantum emitter

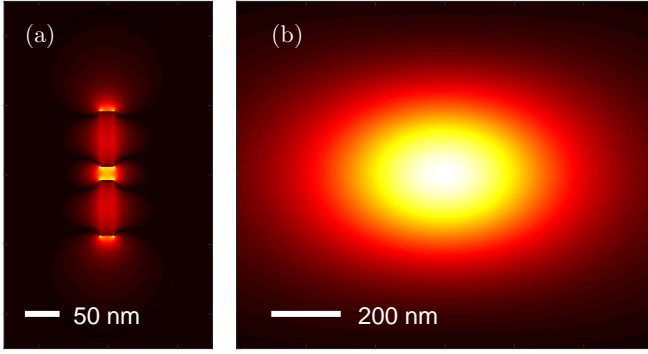


FIG. 6. Spatial map of the detected Stokes intensity from the R6G molecule coupled to the Gold dimer, (a) when the molecule is moved around the and the detector is fixed at 500 nm away from the dimer to the right, (b) when the molecule is fixed at the middle of the dimer gap and the detector is scanned at a plane parallel to the longitudinal axis of the dimer and 500 away from it. Nonlinear scaling of the values are done for visualization purposes.

placed nearby. As seen, in this case, it may be desired for the molecule to be placed in the middle of the dimer gap in order for the Raman response to be optimized. In contrast, for a fixed molecule location, one might want to move the detector around and scan for the maximum intensities. The detector location dependence of the Stokes signal is plotted in Fig. 6(b) where a dipole emission in the far field is seen. As mentioned before, such spatial maps can be produced as easily for other plasmonic geometries such as waveguides, without any need to modify our theory. All one needs, is an accurate representation of the total system Green function that in our case was made available through use of QNMs.

#### IV. CONCLUSIONS

We have developed a powerful and intuitive Green function based formalism that can be used to model

SERS using plasmonic systems of arbitrary geometry. For example, the plasmonic environment can be either a resonator, a waveguide, or even a more complex structure such as a hybrid photonic-plasmonic platform. A generalized master equation is employed such that the plasmonic environment is treated as a system bath and the system dynamics are projected onto the basis of the molecular vibrations. Therefore, while the plasmonic degrees of freedom are not present, the exact system Green function is self-consistently incorporated to account for true plasmonic characteristic such as emission enhancement and quenching. As a result, analytical expressions in the most general form are given for the SERS spectrum near plasmonic environments that can be used to quantify Stokes and anti-Stokes emission intensities. We reported that the dynamics of the SERS is quite different in generation stage than in propagation stage. The induced Raman polarization seems to be emitting photons at Stokes frequency proportional to the plasmonic enhancement at the co-existing anti-Stokes frequency and vice-versa. However, plasmonic LDOS comes into play differently at propagation stage such that both Stokes and anti-Stokes photons are enhanced at their respective frequencies. In comparison to the excising models mostly working in a single mode regime, our model simply extends beyond this limitation and characterizes the Raman spectrum as a function of detuning, pump power, spatial location of the molecule/detector etc. Given the analytical nature of our results, it can be used to model any SERS experiment in no time, once the system Green function is accurately available.

#### ACKNOWLEDGMENT

We thank Queen's University and the Natural Sciences and Engineering Research Council of Canada for financial support. We would also like to thank Amr Helmy, Herman M. K. Wong and Reuven Gordon for useful discussions.

- 
- [1] S. Nie and S. R. Emory, *Science* **275**, 1102 (1997).
  - [2] S. Lal, S. Link, and N. J. Halas, *Nat Photon* **1**, 641 (2007).
  - [3] S. A. Maier, *Plasmonics: Fundamentals and Applications* (Springer, 2007).
  - [4] E. C. L. Ru and P. G. Etchegoin, *Principles of Surface-Enhanced Raman Spectroscopy* (Elsevier, 2009).
  - [5] R. Zhang, Y. Zhang, Z. C. Dong, S. Jiang, C. Zhang, L. G. Chen, L. Zhang, Y. Liao, J. Aizpurua, Y. Luo, J. L. Yang, and J. G. Hou, *Nature* **498**, 82 (2012).
  - [6] P. Alonso-González, P. Albella, M. Schnell, J. Chen, F. Huth, A. Garcia-Etxarri, F. Casanova, F. Golmar, L. Arzubíaga, L. Hueso, J. Aizpurua, and R. Hillenbrand, *Nature Communications* **3**, 684 (2012).
  - [7] S. Yampolsky, D. A. Fishman, S. Dey, E. Hulkko, M. Banik, E. O. Potma, and V. A. Apkarian, *Nat Photon* **8**, 650 (2014).
  - [8] R. Chikkaraddy, B. de Nijs, F. Benz, S. J. Barrow, O. A. Scherman, E. Rosta, A. Demetriadou, P. Fox, O. Hess, and J. J. Baumberg, *Nature* **535**, 127 (2016).
  - [9] Y. Huang, Y. Fang, Z. Zhang, L. Zhu, and M. Sun, *Light: Science & Applications* **3**, e199 (2014).
  - [10] S. J. P. Kress, F. V. Antolinez, P. Richner, S. V. Jayanti, D. K. Kim, F. Prins, A. Riedinger, M. P. C. Fischer, S. Meyer, K. M. McPeak, D. Poulikakos, and D. J. Norris, *Nano Letters* **15**, 6267 (2015).
  - [11] C. Lee, F. Dieleman, J. Lee, C. Rockstuhl, S. A. Maier, and M. Tame, *ACS Photonics* **3**, 992 (2016).

- [12] F. Peyskens, A. Dhakal, P. Van Dorpe, N. Le Thomas, and R. Baets, *ACS Photonics* **3**, 102 (2016).
- [13] M. Barth, S. Schietinger, S. Fischer, J. Becker, N. Nüsse, T. Aichele, B. Löchel, C. Sönnichsen, and O. Benson, *Nano Letters* **10**, 891 (2010).
- [14] M. D. Baaske and F. Vollmer, *Nat Photon* **10**, 733 (2016).
- [15] W. Gu, H. Choi, and K. K. Kim, *The Journal of Physical Chemistry A* **111**, 8121 (2007).
- [16] A. M. Kelley, *The Journal of Chemical Physics* **128**, 224702 (2008).
- [17] D. J. Masiello and G. C. Schatz, *Phys. Rev. A* **78**, 042505 (2008).
- [18] D. J. Masiello and G. C. Schatz, *The Journal of Chemical Physics* **132**, 064102 (2010).
- [19] A. Delfan, M. Liscidini, and J. E. Sipe, *J. Opt. Soc. Am. B* **29**, 1863 (2012).
- [20] J. L. Payton, S. M. Morton, J. E. Moore, and L. Jensen, *Accounts of Chemical Research* **47**, 88 (2014).
- [21] J. R. Lombardi and R. L. Birke, *The Journal of Physical Chemistry C* **118**, 11120 (2014).
- [22] N. S. Mueller, S. Heeg, and S. Reich, *Phys. Rev. A* **94**, 023813 (2016).
- [23] A. F. Koenderink, *Opt. Lett.* **35**, 4208 (2010).
- [24] P. T. Kristensen, C. V. Vlack, and S. Hughes, *Opt. Lett.* **37**, 1649 (2012).
- [25] P. T. Kristensen and S. Hughes, *ACS Photonics* **1**, 2 (2014).
- [26] C. Sauvan, J. P. Hugonin, I. S. Maksymov, and P. Lalanne, *Phys. Rev. Lett.* **110**, 237401 (2013).
- [27] P. Roelli, N. Piro, and T. J. Kippenberg, *Nat Nano* **11**, 164 (2016).
- [28] M. K. Schmidt, R. Esteban, A. González-Tudela, G. Giedke, and J. Aizpurua, *ACS Nano* **10**, 6291 (2016).
- [29] H. J. Carmichael, *Statistical Methods in Quantum Optics I* (Springer, 2002).
- [30] H.-P. Breuer and F. Petruccione, *The Theory of Open Quantum Systems* (Oxford, 2007).
- [31] A. Kowalewska-Kudlaszyk and R. Tanas, *Journal of Modern Optics* **48**, 347 (2001).
- [32] H. T. Dung, L. Knöll, and D.-G. Welsch, *Phys. Rev. A* **57**, 3931 (1998).
- [33] L. G. Suttorp and A. J. van Wonderen, *EPL (Europhysics Letters)* **67**, 766 (2004).
- [34] L. Novotny and B. Hecht, *Principles of Nano-Optics*, 2nd ed. (Cambridge University Press, 2012).
- [35] R.-C. Ge, C. Van Vlack, P. Yao, J. F. Young, and S. Hughes, *Phys. Rev. B* **87**, 205425 (2013).
- [36] P. Yao, C. Van Vlack, A. Reza, M. Patterson, M. M. Dignam, and S. Hughes, *Phys. Rev. B* **80**, 195106 (2009).
- [37] M. Aspelmeyer, T. J. Kippenberg, and F. Marquardt, *Rev. Mod. Phys.* **86**, 1391 (2014).
- [38] P. T. Leung, S. Y. Liu, and K. Young, *Phys. Rev. A* **49**, 3982 (1994).
- [39] M. Kamandar Dezfouli, R. Gordon, and S. Hughes, *Phys. Rev. A* **95**, 013846 (2017).
- [40] H. Watanabe, N. Hayazawa, Y. Inouye, and S. Kawata, *The Journal of Physical Chemistry B* **109**, 5012 (2005).